Polymer Bulletin (2019) 76:3517–3533
https://doi.org/10.1007/s00289-018-2556-y

ORIGINAL PAPER

DBSA to improve the compatibility, solubility, and infusibility of cellulose nanowhiskers modified by polyaniline in reinforcing a natural rubber-based nanocomposite

Michael Jones Silva[1] · Cicero Rafael Cena[2] · Alex Otávio Sanches[3] · Luiz Henrique Capparelli Mattoso[4] · Jose Antonio Malmonge[3]

Received: 25 June 2018 / Revised: 1 October 2018 / Accepted: 6 October 2018 /
Published online: 15 October 2018

Abstract

In this study, the authors evaluate the potential of the reinforcement of cellulose nanowhiskers coated with polyaniline-DBSA (CNW-PANiDB) in a natural rubber latex nanocomposite. For this purpose, cellulose nanowhiskers (CNWs) were obtained by acid hydrolysis and coated with polyaniline by in situ polymerization in an acidic medium using dodecylbenzenesulfonic acid (DBSA). The nanocomposites based on natural rubber (NR) reinforced with CNW-PANiDB were obtained by a casting/evaporation method. Sample characterization was performed by DC electrical conductivity, thermogravimetric analysis, strain–stress test, UV–Vis–NIR and field emission scanning electron microscope. The UV–Vis–NIR spectrum of the NR/CNW-PANiDB nanocomposite revealed three characteristic absorption peaks around 350, 425, and 830 nm, assigned to PANiDB in emeraldine salt form. The mechanical properties of the nanocomposite, such as Young's modulus and tensile strength, were improved by increasing the amount of CNW-PANiDB. The electrical conductivity of the nanocomposite increased by seven orders of magnitude by adding 10 mass% of CNW-PANiDB. This result indicates that CNWs coated with polyaniline-DBSA are an excellent material for use as mechanical reinforcement and to improve electrical conductivity. Thus, NR/CNW-PANiDB nanocomposite films have potential to be used as anticorrosive, electrostatic discharge, electromagnetic interference shielding materials, transducers, and electroactive materials.

Keywords Natural rubber · Cellulose nanowhiskers · Polyaniline · Nanocomposite · Properties analysis

✉ Michael Jones Silva
michael.silva@unesp.br

Extended author information available on the last page of the article

Introduction

Materials from natural sources have many advantages over synthetics, such as low cost of production, abundant raw material sources, and biodegradable character. Among natural materials, cellulose stands out as the most abundant material in nature and is found in plant, algal, and animal organisms. Cellulose is a homopolymer of high molecular weight composed of repeating units of β-1,4-D-glucopyranose and has, as its main features, low cost, high crystallinity, and mechanical strength [1–3]. Its dimensions may be reduced by breaking the molecular chains (amorphous region) by acid hydrolysis to obtain highly crystalline microfibers (CMF) or nanowhiskers (CNWs) [3, 4]. Advances in cellulose chemistry have made possible the creation of new materials for use in different industrial and technological sectors. Cellulose can be applied to coatings, films, membranes, construction materials, textiles, paper, foodstuff, and pharmaceutical products [5–7].

The use of cellulose fiber as a reinforcement in composites is another area garnering attention in the last decade [8]. Its excellent mechanical properties and reinforcing capacity combined with low manufacturing cost, high surface area, and biodegradability make cellulose an excellent candidate to replace synthetic material reinforcements [9, 10]. In recent decades, a number of studies have demonstrated the potential of cellulose fiber as a reinforcement of several polymeric matrices, such as elastomers [11, 12], thermoplastics [13, 14], and thermosets [15, 16].

The possibility of reducing the dimensions of cellulose fibrils with acid hydrolysis has opened its field of application in nanoscience. CNWs are usually obtained in a stable aqueous suspension owing to the sulfate groups on its surfaces [4, 17]. Stability of the nanofiber dispersion is an important parameter to obtain nanocomposites using water-soluble polymer matrices.

Among the polymeric materials, natural rubber (NR) in the latex form has been extensively used to obtain nanocomposites reinforced with CNW [10, 18]; it is a linear biopolymer with a high molecular mass of the cis-1.4-polyisoprene chain [19]. The superior features of NR such as elasticity, flexibility, and resilience make it one of the most used polymers in the industrial sector (annual production exceeding 12,070 thousand metric tons) [20]. Usually, the rubber industry uses some type of loads (materials organic and/or inorganic), such as silica, carbon black, or calcium carbonate, to improve the performance of the rubber; these materials are derived from non-renewable sources, unlike CNW [21].

Visakh et al. studied the mechanical and thermal properties of a natural rubber nanocomposite reinforced with nanofibers extracted from bamboo residues and observed that the introduction of CNW in the NR matrix had a positive impact on its properties [21]. The dispersion of 10 wt% CNW increased the Young's modulus of the nanocomposite from 1.7 ± 0.2 to 3.8 ± 0.2 MPa. Siqueira et al. used nanofibrils extracted from capim dourado to reinforce the NR matrices and observed that the modulus of the nanocomposite increased to $(1.6 \pm 0.2) \times 10^2$ MPa with the dispersion of 10 wt% of CNW [22]. Similar results were obtained by

Bendahou et al., who used rachis nanofibrils from date palm trees; they observed an increase in the Young's modulus of 0.5 ± 0.2 MPa to $(1.18 \pm 0.06) \times 10^2$ MPa with the addition of 10% wt% CNW [11].

Several studies also have proposed the mixture of CNW with intrinsic conductive polymers (ICPs) to obtain conductive nanocomposites [17, 23–25]. Polyaniline (PANi) is among the most studied intrinsically conductivity polymers (ICPs), owing to its good electrical conductivity, thermal stability, and facile synthesis [26, 27]. PANi can be applied in electromagnetic interference shielding [28], rechargeable batteries [29], conductive adhesives and coatings [30], and sensors [31, 32]. However, there are some limitations that can influence the application of PANi, such as poor infusibility, low solubility in organic solvents, and poor mechanical properties [27, 33]. The solubility and infusibility of the PANi in the host matrix can be improved by using organic acids such as dodecylbenzenesulfonic acid (DBSA) and p-toluenesulfonic acid (PTSA) [17]. These organic acids can also act as dopants, increasing the electrical conductivity of the material [26]. Concerning the mechanical properties, these can be improved by mixing the PANi with a polymeric matrix to obtain composites or blends. Such observations were evidenced by using CNW as a support for PANi, where satisfactory results were achieved, and these studies confirm the good interaction between the two phases [23, 24]. Mattoso et al. performed the in situ polymerization of aniline onto CNW and obtained a flexible CNW-PANi nanocomposite with an electrical conductivity of about 0.01 S/cm [23]. Similar results were obtained by Hu et al. [34] with an electrical conductivity of around 0.05 S/cm and Young's modulus equal to 5.6 GPa.

The reinforcement characteristic of the CNW-PANi nanocomposite dispersed in polymer matrices has also been investigated. Auad et al. analyzed the mechanical and electrical properties of CNW coated with a PANi-reinforced polyurethane (PU) matrix [35]. The authors obtained an improvement in the mechanical properties of PU matrices with the dispersion CNW-PANi, but not in electrical conductivity, due to the dedoping of PANi [35]. Araujo et al. produced polyamide-6 composite reinforced with cellulose fibrils coated with PANi, and the electrical conductivity of the composite was three orders of magnitude higher than that of the neat nylon-6 matrices [36].

The number of studies that have used CNW as a reinforcement in nanocomposites based on natural rubber is relatively large [11, 22, 37]; however, there is [35, 36, 38] no work yet that has used CNW coated with PANi polymerized in acidic DBSA medium to reinforce nanocomposites based on natural rubber. In this sense, the present work proposes a new conductive nanocomposite which is based on natural rubber, reinforced with CNW, coated with PANi obtained via in situ polymerization of the aniline onto CNW in DBSA solution. We evaluated the capacity of DBSA to improve the compatibility, solubility, and infusibility of CNW modified by polyaniline in reinforcement of the NR matrices and its influence on the mechanical, electrical, and thermal properties of the nanocomposites.

Experimental

Materials

Ammonium peroxydisulfate (APS), dodecylbenzenesulfonic acid (DBSA), sulfuric acid, and aniline (distilled under vacuum) were purchased from Sigma-Aldrich. Cotton fibers with a particle size of 50 μm (Sigmacell Cellulose type 50) were purchased from Sigma-Aldrich. Dialysis membranes with the following characteristics: membrane tube, MWCO: 12 to 14.000, 75 mm flat width, vol/length = 18 mL/cm, length = 15 mm, were purchased from Spectra/Por dialysis membranes, Houston, TX, USA. Natural rubber (NR) latex was collected from Hevea brasiliensis trees (Clone RIMM 600) in the experimental farm of the São Paulo State University (UNESP), campus of Ilha Solteira, Brazil. The latex was stabilized using a commercial solution of ammonium hydroxide to avoid coagulation. The dry rubber content was determined by standard methods (ISO 124:2014).

Extraction of cellulose nanowhiskers

CNWs were prepared by acid hydrolysis according to the procedure described by Medeiros et al. [39]. Microcrystalline cotton cellulose microfibers were immersed in a sulfuric acid solution (64%w/v) at 45 °C using a ratio of cellulose microfibers to acid solution of 1:7.1 g mL^{-1}. The CNW dispersion was stirred vigorously for 60 min and then quenched in cold water (5 mass equivalents). The resulting dispersion was centrifuged at 10,000 rpm for 10 min at 10 °C to separate the CNW from the acid solution containing hydrolyzed amorphous cellulose chains. The centrifuged cake containing CNW was dispersed in water and centrifuged again. This operation was performed three times, and the final CNW content was dispersed in 250 mL deionized water followed by dialysis against water until reaching a constant pH (4.0).

Preparation of CNW-PANi samples

The CNW-PANi dispersion was prepared by in situ polymerization of aniline onto CNW surfaces according to the procedure described by Silva et al. [17]. The procedure consisted of mixing 16.6 mL of CNW aqueous dispersion (4.3 g/100 mL) and 0.2 mL of aniline in 100 mL of deionized water. This mixture was left under constant stirring for 2 h at a temperature of 5 °C. DBSA was added to the CNW/aniline dispersion, and the mixture was maintained at 35 rpm for 1 h at 5 °C. Finally, a defined amount (0.15 g) of oxidant (APS), dissolved in deionized water, was added to the CNW/aniline/DBSA dispersion to initiate the polymerization. After 12 h, CNW-PANiDB was separated from the reaction media by centrifugation at 7000 rpm for 10 min to eliminate the reaction by-products. The CNW-PANiDB sample was then re-dispersed in water and centrifuged again, and this

procedure was repeated three times, following which the final content was either re-dispersed in water at a desirable concentration (e.g., for characterization) or kept at high concentration.

NR/CNW-PANiDB nanocomposite preparation

The NR/CNW-PANiDB nanocomposite was obtained by incorporation of an aqueous dispersion of CNW-PANiDB in natural rubber latex at desired mass proportions (90/10 and 95/05). The NR/CNW-PANiDB mixture was maintained at constant stirring for 2 h at approximately 20 °C to eliminate bubbles and obtain a homogeneous dispersion of the CNW-PANiDB into NR latex. The mixtures were then cast on glass substrates and dried in a conventional oven at 60 °C for 12 h to obtain films approximately 200 μm thick.

The NR/CNW-PANiHC (HC is hydrochloric acid) and NR/PANiDB samples in the 90/10 mass proportion were obtained using the same methodology as the NR/CNW-PANiDB nanocomposite, for comparison.

Methods

UV–Vis analyses of aqueous CNW-PANiDB dispersions and NR/CNW-PANiDB films were performed using a Cary 50 spectrophotometer (Varian) in the range from 300 to 1100 nm. Thermogravimetric (TG/DTG) measurements were carried out in the temperature range from 25 °C to 600 °C, at a heating rate of 10 °C/min in a nitrogen atmosphere with a flow rate of 60 mL/min using an equipment Q500a model (TA Instruments). Approximately 10 mg was used for each sample. The glass transition temperature (T_g) of the samples (ca. 6 mg) was measured using a TA Instruments Model MDSC 292 with a scan rate of 10 °C/min within the temperature range from − 100 °C to 175 °C, in a nitrogen atmosphere.

A Zeiss field emission scanning electron microscope (FESEM-Supra 35) was used to investigate the morphology of the CNW, CNW-PANiDB, and NR/CNW-PANiDB samples. Separately, 5 μL of CNW (4.3 g/100 mL) and CNW-PANi (5.2/100 mL) aqueous suspension were diluted in 1 mL isopropyl alcohol, and 3 μL of the resultant suspension was cast onto silicon substrates, dried in dynamic vacuum for 1 h at approximately 20 °C, and coated with carbon by sputtering prior to FESEM analysis. The NR/CNW-PANiDB nanocomposites were frozen under liquid nitrogen, fractured, and coated with carbon by sputtering prior to FESEM analysis.

Tensile tests were carried out using an Instron tensometer at a crosshead speed of 500 mm/min and 100 N load cell, following ISO 37:2011. The samples were prepared in the tie form with a 23-mm-long and 4.5-mm-wide neck, whereas the thickness of the samples varied between 200 and 300 μm. Mechanical tests were repeated eight times according to ISO 1286:2006.

Electrical conductivity measurements were carried out using two-probe methods coupled to a voltage/current source of Keithley Instruments model 247 high voltage supply. Gold electrodes were evaporated onto both faces of the films by evaporation.

Results and discussion

Morphological analysis

Morphological analyses of the CNW uncoated and coated with PANiDB were carried out by FESEM and are shown in Fig. 1a, b. The average diameters and length of the CNW are around 36 ± 3 nm and $(3.7 \pm 0.2) \times 10^2$ nm, respectively. Results can be estimated by the aspect ratio (length/diameter) of CNW, whose value was approximately 10; this is similar to the values found in the literature [17, 40]. When the cellulose nanofibrils are coated with PANiDB, the CNW surface appears rough, indicating that PANiDB are formed during in situ polymerization as expected, Fig. 1b [17]. The CNW coating with PANi enables its use as an electrically conductive filler in the reinforcement of the nanocomposite to improve the electrical and mechanical properties of polymeric matrices.

The incorporation of the CNW-PANiDB nanofiller into the polymeric matrices results in an increase in the surface roughness; this fact can be observed in Fig. 2a, b. This was attributed to the formation of a percolative network by CNW-PANiDB to concentrations above the percolation threshold. For CNW-PANiDB, this value should be close to that of CNW, considering a uniform coating and calculated at approximately 5.3% vol% or 8.5 mass% [38] (density of 0.93 and 1.5 g cm^{-3} for NR and CNW, respectively [41, 42]). The CNW-PANiDB nanofiller was homogeneously dispersed throughout the NR matrix. A good interaction between CNW-PANiDB and NR was also observed, as evinced by the absence of holes in the matrix and around CNW-PANiDB (Fig. 2b); this is an excellent indication of good interaction between the phases. This behavior was not observed with the NR/CNW-PANiHC nanocomposite (Fig. 2c, d); there are many holes on the fractured surface, demonstrating poor interaction between NR and CNW-PANiHC filler.

Optical analysis

The presence of PANiDB on the CNW as well as its oxidation state in the CNW-PANiDB and NR/CNW-PANiDB nanocomposite was investigated through

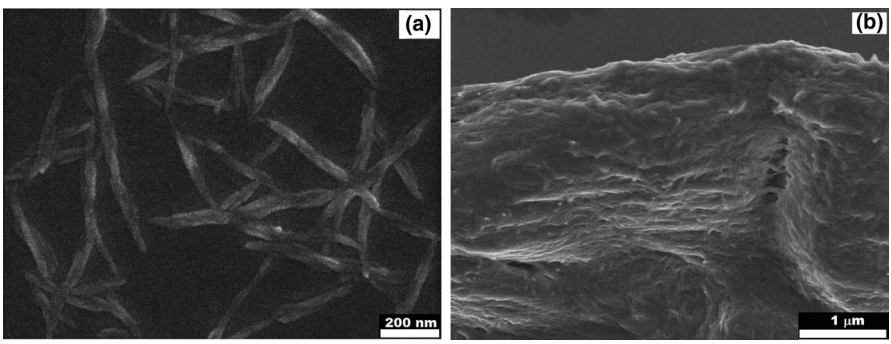

Fig. 1 FESEM analysis of **a** CNW and **b** CNW-PANiDB

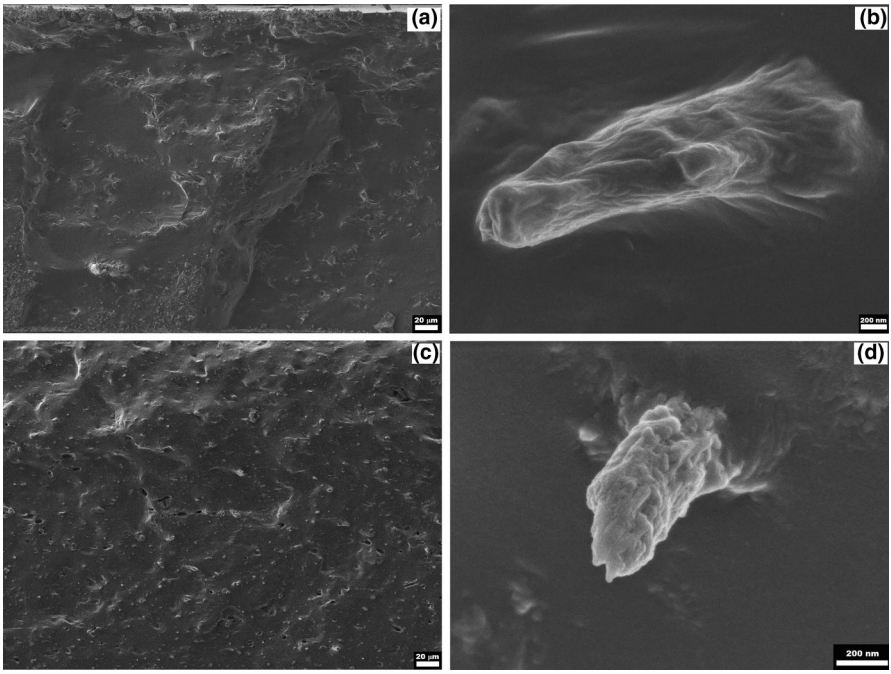

Fig. 2 FESEM analysis of the cryofractured surface of the **a**, **b** NR/CNW-PANiDB and **c**, **d** NR/CNW-PANiHC nanocomposite reinforced with 10 mass% of filler

UV–Vis–NIR analysis. Figure 3a, b shows the UV–Vis–NIR absorption spectra of the PANiDB and CNW-PANiDB dispersion and NR/CNW-PANiDB nanocomposite film (in proportion of 90/10 and 95/05 wt/wt), respectively.

Characteristic absorption peaks of PANiDB in the emeraldine salt form were observed in the UV–Vis–NIR spectrum of the CNW-PANiDB and PANiDB dispersion at around 350, 425, and 760 nm. The absorption peaks at 425 and 760 nm

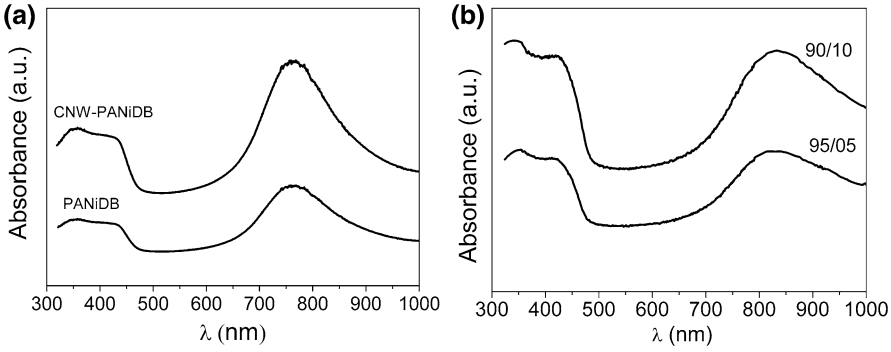

Fig. 3 UV–Vis–NIR spectra of the **a** PANiDB and CNW-PANiDB, and **b** NR/CNW-PANiDB nanocomposites

are assigned to the polaron-π^* transition and π-polaron transition, respectively. The absorption peak appearing at around 350 nm can be ascribed to the π–π^* transition of the benzenoid rings [43–45]. The same absorption peaks of PANiDB were detected in the UV–Vis–NIR spectrum of the NR/CNW-PANiDB nanocomposites at 350, 425, and 830 nm (Fig. 3b). The absorbance ratio of the polaron band (760 to 830 nm) to the benzenoid π–π^* electron transition (340–370 nm) can be used to estimate the level of PANi doping [46]. The estimated values were 1.42, 0.99, and 0.95 for CNW-PANiDB, NR/CNW-PANiDB (90/10), and NR/CNW-PANiDB (95/05), respectively. The lower absorbance ratio for the NR composites indicates that PANiDB undergoes slight dedoping when it is incorporated in the matrix. When preparing the nanocomposites, the pH of the CNW-PANiDB dispersion was approximately 3.0, while that of the NR latex was adjusted to 7.0. We believe that during mixing, dedoping of the PANiDB may occur. On the other hand, the displacement of the peak is associated with the conformation of the PANiDB chains. According to Laska [47], the polyaniline conformation chain in polymer blends is influenced by several factors, such as the chemical nature of a dopant, molar ratio of dopant to PANi, and the solvent and polymer matrix in a blend. In our case, the peak attributed to the π-polaron transition displaced to a higher wavelength (760 to 860 nm), indicating that the PANiDB chain is more extended in the nanocomposite. Similar behavior was observed by Job et al. [48] using Raman spectroscopy, which was attributed to the chemical interaction between NR and PANi.

Thermal analysis

TG/DTG curves of the neat samples and nanocomposites are shown in Fig. 4a and b, respectively. TG/DTG curves for PANiDB show two ranges of mass loss with intense peaks at 287 °C (76% mass loss) and 483 °C (12% mass loss), assigned to the degradation and evaporation of DBSA, and the structural degradation of PANiDB, respectively [43, 49]. NR showed three main stages of degradation: the first located between 25 and 127 °C was attributed to the loss of water in the sample; the second, between 164 and 292 °C, was due to the simultaneous decomposition

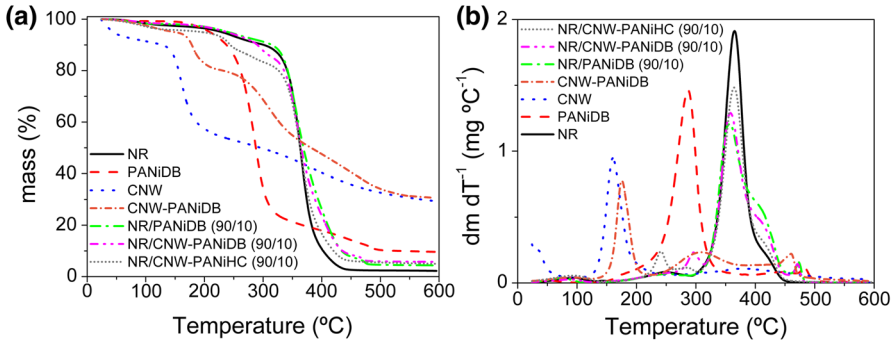

Fig. 4 **a** TGA and **b** DTGA curves of neat NR, CNW, PANiDB, CNW-PANiDB, NR/PANiDB (90/10), NR/CNW-PANiHC (90/10) and NR/CNW-PANi (90/10) samples

of some lipids and fatty acids, or even reticulation and chain cleavage [50, 51]; the third, and more intense, located between 300 and 460 °C, corresponded to the structural decomposition of NR in nitrogen atmosphere [50, 51]. The shoulder observed at 420 °C was associated with the slow decomposition of polymer chains or highly cross-linked residues [52]. Three mass loss events were observed for CNW: the first, below 150 °C, was attributed to water evaporation (8% mass loss); the second, from 150 to 210 °C (36 mass%), was assigned to cellulose degradation (characteristic of highly hydrolyzed cellulose); and the third, between 250 and 450 °C (23 mass%), was attributed to CNW degradation from regions that were less-exposed during acidic hydrolysis [40, 53]. The CNW-PANiDB nanocomposites exhibited higher thermal stability than CNW. The PANiDB deposited on CNW is a more thermally stable component and acts as a protective barrier against thermal degradation [50]. The NR/PANiDB TG profile was similar to that of NR, demonstrating that the PANiDB did not negatively affect the thermal stability of the NR in order to catalyze degradation processes due to the presence of the dopant.

The NR/CNW-PANiDB nanocomposites typically presented five main degradation stages, owing to the superposition of the processes for individual phases. The first stage (30–125 °C) was attributed to water loss, the second (175–292 °C) to the thermal decomposition of lipids and fatty acids [46, 47], the third (270–316 °C) to the superposition of the CNW and PANiDB degradation processes, and the fourth (300–460 °C) and fifth (456–486 °C) stages to the structural decomposition of degraded NR and PANiDB, respectively. The NR/CNW-PANiHC nanocomposite showed the first weight loss before 130 °C owing to the loss of water and secondary dopant (a fraction of the total HCl content). Two other peaks were observed between 160–261 °C and 255–305 °C, which were primarily attributed to the thermal decomposition of lipids and fatty acid, and acid evaporation, respectively. Above 300 °C, the curve profile was similar to that of NR.

Figure 5 shows the DSC analysis of the elastomer nanocomposites based on natural rubber reinforcement with CNW-PANiDB, CNW-PANiHC and PANiDB and the effect of the addition of fillers on the matrix glass transition temperature (T_g). The

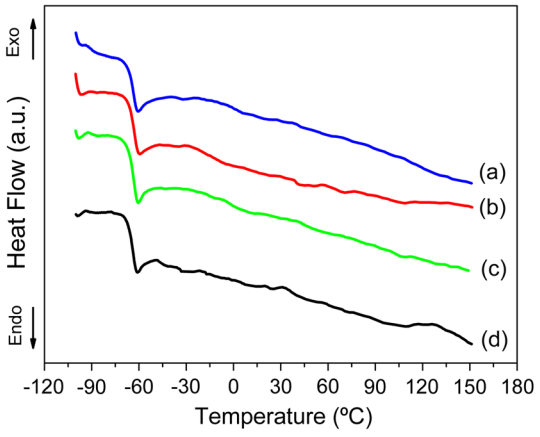

Fig. 5 DSC curves of the samples **a** neat NR, **b** NR/PANiDB, **c** NR/CNW-PANiDB and **d** NR/CNW-PANiHC, all sample with 10 mass% of filler

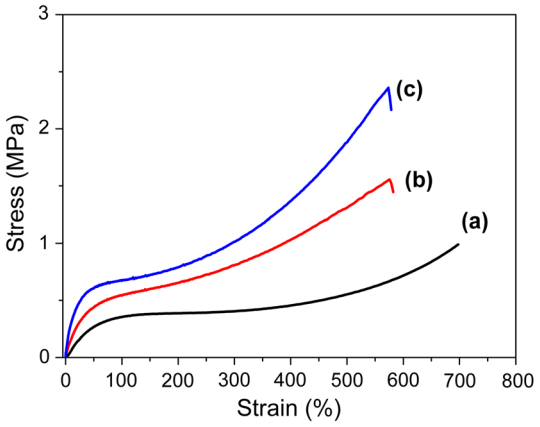

Fig. 6 Stress–strain curves of the samples **a** neat NR, **b** NR/CNW-PANiDB (95/05), and **c** NR/CNW-PANiDB (90/10)

Table 1 Young's modulus (Y), tensile strength (σ_r), and elongation (ε_r) at break of the composite films and neat NR

Samples	Y (Mpa)	σ_r (Mpa)	ε_r (%) 10^2
NR (100/0)	0.68 ± 0.05	1.36 ± 0.04	7.00 ± 0.09
NR/CNW-PANiDB (95/05)	1.3 ± 0.1	1.7 ± 0.2	6.4 ± 0.4
NR/CNW-PANiDB (90/10)	3.9 ± 0.3	2.8 ± 0.2	5.9 ± 0.2
NR/CNW-PANihc (90/10)	1.7 ± 0.4	1.2 ± 0.1	5.6 ± 0.2
NR/PANiDB (90/10)	1.5 ± 0.2	3.0 ± 0.1	6.8 ± 0.1
NR/CNW (90/10)	8.2 ± 0.9	3.4 ± 0.3	3.9 ± 0.1

DSC curve analysis showed no significant effect of the fillers on natural rubber T_g which was locate around −64 °C. This result is in accordance with other works in the literature where no modification of natural rubber T_g values was reported regardless of the nature of fillers [54–58].

Mechanical tests

Figure 6 compares the typical stress–strain characteristic curves of elastomeric materials for the NR/CNW-PANiDB nanocomposite with 5% and 10 wt% of CNW-PANiDB and NR [33]. The addition of CNW-PANiDB in a proportion of 5–10 wt% substantially impacted the mechanical properties of the nanocomposites. This behavior is indicative of the transfer of tension from NR matrices to CNW-PANiDB when the sample experiences an external mechanical stress. Both the Young's modulus and tensile strength significantly increased upon addition of the CNW-PANiDB dispersion into NR, while the rupture strain decreased. For 10 wt% CNW-PANiDB, the tensile strength and Young's modulus were 3.1 ± 0.3 MPa and 3.5 ± 0.1 MPa, respectively, both higher than that of the neat natural rubber (1.36 ± 0.04 MPa and 0.68 ± 0.05 MPa, respectively). The data extracted from the stress–strain curves are presented in Table 1.

The improvement in the mechanical properties of the nanocomposites can be attributed to the phenomenon of mechanical percolation of CNW-PANiDB, which form a continuous network [59, 60]. Thus, CNW-PANiDB acts as a barrier impeding deformation of the NR chains, i.e., the formation of rigid CNW-PANiDB networks facilitates the transfer of stress with CNW-PANiDB. The mechanical percolation is strongly dependent on mechanical factors such as the aspect ratio of the nanoparticle-enhanced rod-like format and the origin of the cellulose [60].

Analysis of Fig. 7 and Table 1 shows that the mechanical properties of the NR/CNW-PANiDB nanocomposite are better than those of the NR/CNW-PANiHC and NR/PANiDB composites. One important factor is the acidic nature employed to obtain the CNW-PANi filler. The DBSA, used in the polymerization process of the PANi onto CNW surface, acts as a surfactant modifying the surface of the CNW improving their compatibility with the NR matrices. In addition, the pH of the CNW-PANiDB suspension before being mixed with NR latex was around 3, higher than that of CNW-PANiHC (pH ~ 1). We believe that since HCl is a stronger acid than DBSA, it can degrade lipids, proteins, and other components that directly affect the properties of the composite [53].

A comparative analysis was also performed between NR/CNW-PANiDB and NR/PANiDB samples. When compared with the NR/CNW-PANiDB, the mechanical properties of the NR/PANiDB composite are poorer than those of the NR/CNW-PANiDB nanocomposite, owing to the lack of nanofibers that form a continuous mechanical network and thus enabling efficient transfer of stress from the matrix to filler.

DC electrical analysis

The dispersion of the CNW-PANiDB into NR matrices, in addition to improving the mechanical properties of natural rubber, may also increase the electrical conductivity (σ_{dc}) of nanocomposites. The experimental values of the dc electrical conductivity (σ_{dc}) of the NR/CNW-PANiDB nanocomposites are presented in Table 2. The introduction of a conductive phase in the insulating matrix can form a conductive

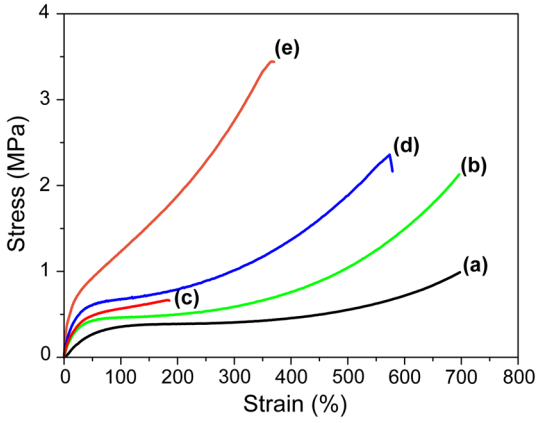

Fig. 7 Stress–strain curves of the samples **a** neat NR, **b** NR/PANiDB, **c** NR/CNW-PANiHC, **d** NR/CNW-PANiDB, and **e** NR/CNW all sample with 10 mass% of filler

Table 2 Electrical conductivity values of neat NR, neat PANiDB, CNW-PANiDB, and NR/CNW-PANiDB nanocomposite films containing different CNW-PANiDB concentrations

Samples	Proportion	σ_{dc} (S/cm)
NR	100/0	$(1.3 \pm 0.3) \times 10^{-14}$
NR/CNW-PANiDB	95/05	$(8.30 \pm 0.04) \times 10^{-11}$
NR/CNW-PANiDB	90/10	$(3.7 \pm 0.1) \times 10^{-7}$
NR/CNW-PANiDB	90/10	$(3.7 \pm 0.1) \times 10^{-9}$
NR/PANiDB	90/10	$(6.9 \pm 0.2) \times 10^{-6}$
CNW-PANiDB	0/100	$(2.1 \pm 0.5) \times 10^{-1}$

path when the concentration of the conductive phase is greater than or equal to the percolation threshold. Conduction in the conductive nanocomposites occurs between the conductive fillers by means of spreading of charge carriers between conductive regions and phonon-assisted tunneling when the distance between the conductive islands is smaller than 20 nm [61, 62]. When the distance between the CNW-PANiDB fillers is sufficiently large, the conductivity is restricted by the presence of the NR matrix, and the spreading of free charge carriers between conductive fillers becomes more difficult. FESEM analysis (Fig. 1a) demonstrates that the CNW presents a rod-like form and an aspect ratio approximately equal to 10 (diameter 40 nm and length 450 nm); in this case, the percolation threshold is approximately 5.3% vol or 8.5 mass% (density of 0.93 and 1.5 g cm^{-3} for NR and CNW, respectively) [63]. For 10 mass% of CNW-PANiDB content dispersed in the nanocomposite in the range of the physical contact percolation threshold, it is expected that the electrical conductivity of the nanocomposite would be similar to that of CNW-PANi, however, the sample with 10 mass% of CNW-PANiDB presents a lower σ_{dc} value. This behavior can be attributed to the partial dedoping of PANi due to the basic pH of NR latex.

The results presented in Table 2 demonstrate that when the amount of CNW-PANiDB is raised in the nanocomposite, the electrical conductivity increases by approximately seven orders of magnitude compared to neat NR. When we performed a comparative analysis between the NR/CNW-PANiHC and NR/CNW-PANiDB nanocomposites, we observed that dedoped PANi occurred more frequently in samples doped with HCl; therefore, samples doped with DBSA demonstrate greater effectiveness in the final electrical properties of the composites.

A comparative analysis performed between the nanocomposites obtained in this paper and in previous studies is presented in Table 3. The NR/CNW-PANiDB

Table 3 Comparative analyses between NR/CNW-PANiDB nanocomposite and composites reinforced with CNW-PANi in previous studies

Samples	σ_{dc} (S/cm)	E (MPa)	σ_r (MPa)	ε_r (%) 10^2	References
PU/CNW-PANiHC	2.2×10^{-10}	31.01 ± 2.35	1.5 ± 0.2	7.5 ± 0.2	Auad et al. [35]
PA-6/CF-PANiTS	6.6×10^{-8}	680 ± 50	53 ± 12	0.4 ± 0.2	Araujo et al. [36]
NR/CNW-PANiDB	3.7×10^{-7}	3.90 ± 0.30	2.8 ± 0.2	5.9 ± 0.2	Present work

nanocomposite possesses superior electrical properties than in other samples reinforced with CNW-PANi in previous studies. As the composites of the previous studies demonstrate, CNW does not fully lose its reinforcement characteristic value when it is covered with PANi, showing its potential for the reinforcement of polymeric matrices.

The electrical and mechanical properties of the nanocomposite obtained in this study presented the same behavior as samples in previous studies, i.e., dc electrical conductivity, and Young's modulus improved with an increase in CNW-PANi quantity into the matrices. This can be attributed to the choice of organic acid in the polymerization of PANi on CNW, such as DBSA, which improved the compatibility, solubility, and infusibility of the PANi with the polymer matrices [33, 64].

The influence of the acid chosen to polymerize the PANi onto CNW also influenced the electrical conductivity of the NR/CNW-PANi nanocomposite, as observed in the data in Table 2. The CNW-PANiHC dispersion suffered greater dedoping when dispersed in the NR matrix because of the higher pH of NR latex. Conversely, the NR/PANiDB composite and NR/CNW-PANiDB nanocomposite with the weaker acid, DBSA, suffered low dedoping when mixed in NR latex.

Conclusion

Flexible films of the NR/CNW-PANiDB nanocomposite were obtained by dispersion in an NR matrix of coated CNW by in situ polymerization of PANi in DBSA. The mechanical tests revealed that the CNW-PANiDB reinforcement improves the mechanical properties of the NR matrix, whereas DBSA improves the compatibility, solubility, and infusibility of CNW-PANi with the matrix. TG/DTG analysis shows that the neat NR and NR/CNW-PANiDB nanocomposite present approximately the same thermal profile and thermal stability; however, the NR/CNW-PANiDB nanocomposite exhibits three mass loss events characteristics of NR, CNW, and PANiDB. CNW-PANiDB showed promise as a conductive filler. The dispersion of CNW-PANiDB in the NR matrix increased its electric conductivity by seven orders of magnitude in relation to neat NR. CNW-PANi forms a conductive three-dimensional network of percolation in the matrix, through which the charge carriers move under the action of an external electric field. Results demonstrated that the in situ polymerization of PANi on CNW in DBSA medium opens novel applications for this material to obtain new nanocomposites and apply them in electronics and in pressure sensors.

Acknowledgements The authors acknowledge the CNPq (Conselho Nacional de Desenvolvimento Científico e Tecnológico) for financial support.

References

1. Deepa B, Abraham E, Cherian BM et al (2011) Structure, morphology and thermal characteristics of banana nano fibers obtained by steam explosion. Bioresour Technol 102(2):1988–1997. https://doi.org/10.1016/j.biortech.2010.09.030

2. Fahma F, Iwamoto S, Hori N et al (2011) Effect of pre-acid-hydrolysis treatment on morphology and properties of cellulose nanowhiskers from coconut husk. Cellulose 18:443–450. https://doi.org/10.1007/s10570-010-9480-0
3. Morán JI, Alvarez VA, Cyras VP, Vázquez A (2008) Extraction of cellulose and preparation of nanocellulose from sisal fibers. Cellulose 15:149–159. https://doi.org/10.1007/s10570-007-9145-9
4. Rosa MF, Medeiros ES, Malmonge JA et al (2010) Cellulose nanowhiskers from coconut husk fibers: effect of preparation conditions on their thermal and morphological behavior. Carbohydr Polym 81:83–92
5. Habibi Y, Lucia LA, Rojas OJ (2010) Cellulose nanocrystals : chemistry, self-assembly, and applications. Cellulose. https://doi.org/10.1007/s10570-006-9061-4
6. Klemm D, Kramer F, Moritz S et al (2011) Nanocelluloses: a new family of nature-based materials. Angew Chemie - Int Ed 50:5438–5466. https://doi.org/10.1002/anie.201001273
7. Khanjanzadeh H, Behrooz R, Bahramifar N et al (2018) Surface chemical functionalization of cellulose nanocrystals by 3-aminopropyltriethoxysilane. Int J Biol Macromol 106:1288–1296. https://doi.org/10.1016/j.ijbiomac.2017.08.136
8. Lu P, Lo Hsieh Y (2010) Preparation and properties of cellulose nanocrystals: rods, spheres, and network. Carbohydr Polym 82:329–336. https://doi.org/10.1016/j.carbpol.2010.04.073
9. Azizi Samir MAS, Alloin F, Dufresne A (2005) Review of recent research into cellulosic whiskers, their properties and their application in nanocomposite field. Biomacromol 6:612–626. https://doi.org/10.1021/bm0493685
10. Siqueira G, Abdillahi H, Bras J, Dufresne A (2010) High reinforcing capability cellulose nanocrystals extracted from Syngonanthus nitens (Capim Dourado). Cellulose 17:289–298. https://doi.org/10.1007/s10570-009-9384-z
11. Bendahou A, Kaddami H, Dufresne A (2010) Investigation on the effect of cellulosic nanoparticles' morphology on the properties of natural rubber based nanocomposites. Eur Polym J 46:609–620. https://doi.org/10.1016/j.eurpolymj.2009.12.025
12. Faruk O, Bledzki AK, Fink H-P, Sain M (2014) Progress report on natural fiber reinforced composites. Macromol Mater Eng 299:9–26. https://doi.org/10.1002/mame.201300008
13. Farahbakhsh N, Shahbeigi-Roodposhti P, Sadeghifar H et al (2017) Effect of isolation method on reinforcing capability of recycled cotton nanomaterials in thermoplastic polymers. J Mater Sci 52:4997–5013. https://doi.org/10.1007/s10853-016-0738-2
14. Farahbakhsh N, Roodposhti PS, Ayoub A et al (2015) Melt extrusion of polyethylene nanocomposites reinforced with nanofibrillated cellulose from cotton and wood sources. J Appl Polym Sci. https://doi.org/10.1002/app.41857
15. Wu GM, Liu D, Liu GF et al (2015) Thermoset nanocomposites from waterborne bio-based epoxy resin and cellulose nanowhiskers. Carbohydr Polym 127:229–235. https://doi.org/10.1016/j.carbpol.2015.03.078
16. Wang WJ, Wang WW, Shao ZQ (2014) Surface modification of cellulose nanowhiskers for application in thermosetting epoxy polymers. Cellulose 21:2529–2538. https://doi.org/10.1007/s10570-014-0295-2
17. Silva MJ, Sanches AO, Malmonge LF et al (2012) Conductive nanocomposites based on cellulose nanofibrils coated with polyaniline-DBSA via in situ polymerization. Macromol Symp. https://doi.org/10.1002/masy.201100156
18. Silva MJ, Soares VO, Dias GC et al (2018) Study of thermal and mechanical properties of a biocomposite based on natural rubber and 45S5 Bioglass® particles. J Therm Anal Calorim. https://doi.org/10.1007/s10973-016-5933-5
19. Medeiros ES, Galiani PD, Moreno RMB et al (2010) A comparative study of the non-isothermal degradation of natural rubber from Mangabeira (Hancornia speciosa Gomes) and Seringueira (Hevea brasiliensis). J Therm Anal Calorim 10:1045–1050
20. Ahmad N, Dayana SAS, Abnisa F, Mohd WAWD (2018) Natural rubber, a potential alternative source for the synthesis of renewable fuels via Hydrous Pyrolysis. IOP Conf Ser Mater Sci Eng 334:012004. https://doi.org/10.1088/1757-899X/334/1/012004
21. Visakh PM, Thomas S, Oksman K, Mathew AP (2012) Crosslinked natural rubber nanocomposites reinforced with cellulose whiskers isolated from bamboo waste: processing and mechanical/thermal properties. Compos Part A Appl Sci Manuf 43:735–741. https://doi.org/10.1016/j.compositesa.2011.12.015

22. Siqueira G, Tapin-Lingua S, Bras J et al (2011) Mechanical properties of natural rubber nanocomposites reinforced with cellulosic nanoparticles obtained from combined mechanical shearing, and enzymatic and acid hydrolysis of sisal fibers. Cellulose 18:57–65
23. Mattoso LHC, Medeiros ES, Baker DA et al (2009) Electrically conductive nanocomposites made from cellulose nanofibrils and polyaniline. J Nanosci Nanotechnol 9:2917–2922. https://doi.org/10.1166/jnn.2009.dk24
24. Latonen R-M, Määttänen A, Ihalainen P et al (2017) Conducting ink based on cellulose nanocrystals and polyaniline for flexographical printing. J Mater Chem C. https://doi.org/10.1039/c7tc03729e
25. Namazi H, Baghershiroudi M, Kabiri R (2017) Preparation of electrically conductive biocompatible nanocomposites of natural polymer nanocrystals with polyaniline via in situ chemical oxidative polymerization. Polym Compos 38:E49–E56. https://doi.org/10.1002/pc.23943
26. Soares BG, Leyva ME, Barra GMO, Khastgir D (2006) Dielectric behavior of polyaniline synthesized by different techniques. Eur Polym J 42:676–686. https://doi.org/10.1016/j.eurpolymj.2005.08.013
27. Bhadra S, Khastgir D, Singha NK, Lee JH (2009) Progress in preparation, processing and applications of polyaniline. Prog Polym Sci 34:783–810. https://doi.org/10.1016/j.progpolymsci.2009.04.003
28. Marins JA, Soares BG, Fraga M et al (2014) Self-supported bacterial cellulose polyaniline conducting membrane as electromagnetic interference shielding material: effect of the oxidizing agent. Cellulose 21:1409–1418. https://doi.org/10.1007/s10570-014-0191-9
29. Simotwo SK, Kalra V (2016) Polyaniline-based electrodes: recent application in supercapacitors and next generation rechargeable batteries. Curr Opin Chem Eng 13:150–160
30. Liu DY, Sui GX, Bhattacharyya D (2014) Synthesis and characterisation of nanocellulose-based polyaniline conducting films. Compos Sci Technol 99:31–36. https://doi.org/10.1016/j.compscitech.2014.05.001
31. Fratoddi I, Venditti I, Cametti C, Russo MV (2015) Chemiresistive polyaniline-based gas sensors: a mini review. Sensors Actuators B Chem 220:534–548
32. Cena CR, Malmonge LF, Malmonge JA (2016) Layer-by-layer thin films of polyaniline alternated with natural rubber and their potential application as a chemical sensor. J Polym Res. https://doi.org/10.1007/s10965-016-1170-7
33. Da Silva MJ, Sanches AO, Malmonge LF, Malmonge JA (2014) Electrical, mechanical, and thermal analysis of natural rubber/polyaniline-Dbsa composite. Mater Res. https://doi.org/10.1590/s1516-14392014005000065
34. Hu W, Chen S, Yang Z et al (2011) Flexible electrically conductive nanocomposite membrane based on bacterial cellulose and polyaniline flexible electrically conductive nanocomposite membrane based on bacterial cellulose and polyaniline. J Phys Chem B. https://doi.org/10.1021/jp204422v
35. Auad ML, Richardson T, Orts WJ et al (2011) Polyaniline-modified cellulose nanofibrils as reinforcement of a smart polyurethane. Polym Int 60:743–750
36. Araujo JR, Adamo CB, De Paoli MA (2011) Conductive composites of polyamide-6 with polyaniline coated vegetal fiber. Chem Eng J 174:425–431
37. Chuayjuljit S, Su-Uthai S, Tunwattanaseree C, Charuchinda S (2009) Preparation of microcrystalline cellulose from waste-cotton fabric for biodegradability enhancement of natural rubber sheets. J Reinf Plast Compos 28:1245–1254. https://doi.org/10.1177/0731684408089129
38. Wu X, Lu C, Xu H et al (2014) Biotemplate synthesis of polyaniline@cellulose nanowhiskers/natural rubber nanocomposites with 3D hierarchical multiscale structure and improved electrical conductivity. ACS Appl Mater Interfaces 6:21078–21085. https://doi.org/10.1021/am505924z
39. Medeiros ES, Mattoso LHC, Ito EN et al (2008) Electrospun nanofibers of poly(vinyl alcohol) reinforced with cellulose nanofibrils. J Biobased Mater Bioenergy 2:231–242
40. Martins MA, Teixeira EM, Corrêa AC et al (2011) Extraction and characterization of cellulose whiskers from commercial cotton fibers. J Mater Sci 46:7858–7864
41. Hervy M, Santmarti A, Lahtinen P et al (2017) Sample geometry dependency on the measured tensile properties of cellulose nanopapers. Mater Des 121:421–429. https://doi.org/10.1016/j.matdes.2017.02.081
42. Parambath Kanoth B, Claudino M, Johansson M et al (2015) Biocomposites from natural rubber: synergistic effects of functionalized cellulose nanocrystals as both reinforcing and cross-linking agents via free-radical thiol-ene chemistry. ACS Appl Mater Interfaces 7:16303–16310. https://doi.org/10.1021/acsami.5b03115

43. Han MG, Cho SK, Oh SG, Im SS (2002) Preparation and characterization of polyaniline nanoparticles synthesized from DBSA micellar solution. Synth Met 126:53–60. https://doi.org/10.1016/S0379-6779(01)00494-5
44. Chen CH (2002) Thermal studies of polyaniline doped with dodecyl benzene sulfonic acid directly prepared via aqueous dispersions. J Polym Res 9:195–200. https://doi.org/10.1023/A:1021395726060
45. Chen CH, Kan YT, Mao CF et al (2013) Fabrication and characterization of water-based polyurethane/polyaniline conducting blend films. Surf Coat Technol 231:71–76. https://doi.org/10.1016/j.surfcoat.2012.03.056
46. Xia H, Wang Q (2001) Synthesis and characterization of conductive polyaniline nanoparticles through ultrasonic assisted inverse microemulsion polymerization. J Nanoparticle Res 3:401–411. https://doi.org/10.1023/A:1012564814745
47. Laska J (2004) Conformations of polyaniline in polymer blends. J Mol Struct 701:13–18. https://doi.org/10.1016/j.molstruc.2004.05.021
48. Job AE, Constantino CJL, Mendes TSG et al (2003) Effect of natural rubber latex on the conducting state of polyaniline blends determined by Raman spectroscopy. J Raman Spectrosc 34:831–836. https://doi.org/10.1002/jrs.1060
49. Lu X, Yen H, Xu J, He C (2002) Electrical conductivity of polyaniline±dodecylbenzene sulphonic acid complex : thermal degradation and its mechanism. Synth Metals 128:167–178
50. Li S-D, Yu H-P, Peng Z et al (2000) Study on thermal degradation of sol and gel of natural rubber. J Appl Polym Sci Doi: https://doi.org/10.1002/(sici)1097-4628(20000314)75:11%3c1339::aid-app3%3e3.0.co;2-0
51. Cáceres Sandoval AP, Gauthier Maradel P (2012) Análisis termogravimetrico como un nuevo método para la determinación de contenido de sólidos totales (CST) y caucho seco (CCS) del látex. Ion 25:57–65
52. Sircar A (2005) Characterization of isomeric elastomers using thermal analysis. J Therm Anal Calorim 49:2005. https://doi.org/10.1007/BF01987450
53. Roman M, Winter WT (2004) Effect of sulphate groups from sulphuric acid hydrolysis on the thermal degradation behaviour of bacterial cellulose. Biomacromolecules. https://doi.org/10.1021/bm034519+
54. Martins MA, Moreno RMB, McMahan CM et al (2008) Thermooxidative study of raw natural rubber from Brazilian IAC 300 series clones. Thermochim Acta. https://doi.org/10.1016/j.tca.2008.06.001
55. Xu T, Jia Z, Wu L et al (2017) Effect of acetone extract from natural rubber on the structure and interface interaction in NR/CB composites. RSC Adv. https://doi.org/10.1039/c7ra03354k
56. Mahmoud HK (2012) Infrared spectroscopy and thermal stability studies of natural rubber-barium ferrite composites. Adv Chem Eng Sci. https://doi.org/10.4236/aces.2012.23041
57. Bras J, Hassan ML, Bruzesse C et al (2010) Mechanical, barrier, and biodegradability properties of bagasse cellulose whiskers reinforced natural rubber nanocomposites. Ind Crops Prod. https://doi.org/10.1016/j.indcrop.2010.07.018
58. Phomrak S, Phisalaphong M (2017) Reinforcement of Natural Rubber with Bacterial Cellulose via a Latex Aqueous Microdispersion Process. J Nanomater 18:17. https://doi.org/10.1155/2017/4739793
59. Favier V, Canova GR, Shrivastava SC, Cavaillé JY (1997) Mechanical percolation in cellulose whisker nanocomposites. Polym Eng Sci 37:1732–1739. https://doi.org/10.1002/pen.11821
60. Tang L, Weder C (2010) Cellulose whisker/epoxy resin nanocomposites. ACS Appl Mater Interfaces 2:1073–1080. https://doi.org/10.1021/am900830h
61. Strumpler R, Glatz-Reichenbach J (1999) Conducting Polymer Composites. J Electroceram 3:329–346. https://doi.org/10.1023/A:1009909812823
62. Rebeque PV, Silva MJ, Cena CR et al (2017) Analysis of the electrical conduction in percolative nanocomposites based on castor-oil polyurethane with carbon black and activated carbon nanopowder. Polym, Compos
63. Garcia de Rodriguez NL, Thielemans W, Dufresne A (2006) Sisal cellulose whiskers reinforced polyvinyl acetate nanocomposites. Cellulose 13:261–270. https://doi.org/10.1007/s10570-005-9039-7
64. Marins JA, Soares BG, Dahmouche K et al (2011) Structure and properties of conducting bacterial cellulose-polyaniline nanocomposites. Cellulose 18:1285–1294. https://doi.org/10.1007/s10570-011-9565-4

Affiliations

Michael Jones Silva[1] · Cicero Rafael Cena[2] · Alex Otávio Sanches[3] · Luiz Henrique Capparelli Mattoso[4] · Jose Antonio Malmonge[3]

[1] Universidade Estadual Paulista (UNESP), Câmpus Experimental de Rosana, Avenida dos Barrageiros, 1.881, Centro, Rosana, SP 19274-000, Brazil

[2] Instituto de Física, Av. Costa e Silva, Bairro Universitário, Universidade Federal. do Mato Grosso do Sul (UFMS), Campo Grande, MS 79070-900, Brazil

[3] Faculdade de Engenharia, Universidade Estadual Paulista (UNESP), Câmpus de Ilha Solteira, Avenida Brasil, 56, Centro, Ilha Solteira, SP 15385-000, Brazil

[4] Laboratório Nacional de Nanotecnologia para o Agronegócio, Embrapa Instrumentação Agropecuária, Rua XV de novembro, 1.452, Centro, São Carlos, SP 13560-970, Brazil